Ingle, R., Roberts, G., Roettger, K., Marroux, H., Sönnichsen, F., Yang, M., Szyc, Ł., Harabuchi, Y., Maeda, S., Temps, F., & Orr-Ewing, A. (2018). Resolving the excited state relaxation dynamics of guanosine monomers and hydrogen-bonded homodimers in chloroform solution. *Chemical Physics*, *515*, 480-492. https://doi.org/10.1016/j.chemphys.2018.07.014

Resolving the Excited State Relaxation Dynamics of Guanosine Monomers and Hydrogen-Bonded Homodimers in Chloroform Solution

Rebecca A. Ingle[1], Gareth M. Roberts[1], Katharina Röttger[1,2], Hugo J. B. Marroux[1], Frank D. Sönnichsen[3], Ming Yang[4], Łukasz Szyc[4], Yu Harabuchi[5], Satoshi Maeda[5], Friedrich Temps[2], and Andrew J. Orr-Ewing[1]*

[1] *School of Chemistry, University of Bristol, Cantock's Close, Bristol, BS8 1TS, UK*

[2] *Institut für Physikalische Chemie, Christian-Albrechts-Universität zu Kiel, Olshausenstraße 40, D-24098 Kiel, Germany*

[3] *Otto Diels Institut für Organische Chemie, Christian-Albrechts-Universität zu Kiel, Otto-Hahn-Platz-4, D-24098 Kiel, Germany*

[4] *Max Born Institut für Nichtlineare Optik und Kurzzeitspektroskopie, Max Born Straße 2A, D-12489 Berlin, Germany*

[5] *Department of Chemistry, Faculty of Science, Hokkaido University, Sapporo 060-0810, Japan*

*Correspondence to: a.orr-ewing@bristol.ac.uk

Abstract: The relaxation pathways of silyl-modified guanosine nucleoside monomers (G) and double-hydrogen-bonded homodimers (GG1) are compared in chloroform solution after 260-nm ultraviolet excitation. Transient absorption spectra support two previously reported relaxation pathways for the monomer with time constants of 210 ± 20 fs and 2.6 ± 0.1 ps. These pathways are associated with bifurcated approach to a seam of conical intersections between the excited $^1\pi\pi^*$ ^1L_a state and the ground electronic state. In the homodimer, an increase in the larger time constant to 18 ± 2 ps is attributed to slower passage through the minimum energy region of the $^1\pi\pi^*$ state. A further time constant of 70 ± 10 fs indicates wavepacket evolution out of the $^1\pi\pi^*$ state Franck-Condon region. A slow component of recovery of ground-state GG1 is proposed to result either from relaxation of the product of inter-base electron-driven proton transfer, or from the lowest triplet state ($^3\pi\pi^*$, T_1).

1. Introduction

The four canonical DNA nucleobases display a remarkable resistance to photochemical damage following the absorption of ultraviolet (UV) radiation. In recent decades, the phenomena that give rise to the photostability of individual bases have been studied in detail,

both experimentally[1,2] and theoretically.[3,4] It is now broadly accepted to be a result of ultrafast non-radiative relaxation of UV populated electronically excited state(s) back to the electronic ground state (S_0), enabled by non-adiabatic dynamics through a range of conical intersections.[4] However, upon being embedded in higher order structural architectures, such as DNA duplexes, the bases are subjected to additional chemical interactions, which have the capacity to both open new (sometimes undesirable) relaxation channels[2,5] and modify the intrinsic photochemistry already inherent to the individual bases.[2,6] Among the most important are intra-strand π-stacking of nucleobases, giving rise to the formation of long-lived excimer/exciplex states,[7,8] and inter-strand hydrogen(H)-bonding, which facilitates ultrafast electron-driven proton transfer (EDPT) across the intermolecular H-bonds of Watson-Crick paired bases.[9-12] With regard to the latter interactions, guanine (Fig. 1, R = H) stands apart from the other canonical nucleobases for its potential to form multiple H-bonds with one or more additional guanine molecules (or other nucleobases). This behaviour is best exemplified by DNA base sequences that are rich in guanine, which arrange into distinct quadruplex (G_4-DNA) structures in eukaryotic telomeres,[13-16] rather than the common double helix motif, and play an indispensable role in replicating the ends of linear chromosomes.[17,18] Moreover, in transfer RNA, H-bonded guanine homodimers are also known to be vital for replication and transcription processes.[19,20] With this behaviour in mind, here we aim to understand how the photochemistry of the guanosine nucleoside (G, Fig. 1) is affected by self-associated H-bonding, in particular dimerization, when compared to the individual G monomer.

The excited state relaxation dynamics of the G monomer have previously been studied in detail in a variety of different solvents[12,21,22] and, more recently, as an isolated species in the gas phase.[23] In general, these measurements indicate that, irrespective of the solvation environment, the dynamics remain qualitatively similar; after excitation between 260 – 270 nm a bi-exponential decay of the excited state population dominates and is completed within ~4 ps.[12,23] The exception to this behaviour occurs in aqueous solution, where only a single time constant of 540–700 fs is observed.[21,22] Theoretical calculations on the simpler guanine nucleobase in the gas phase[24-30] indicate that following initial excitation to the lowest energy, optically bright $^1\pi\pi^*$ (^1L_a) state, population in the vertical Franck-Condon (vFC) region bifurcates into two different relaxation channels, ultimately leading to two

different conical intersection structures located at different points along a continuous seam of $^1L_a/S_0$ degeneracy. Both surface crossing regions involve out-of-plane ring deformation at the C2 position (see Fig. 1). Dynamics simulations by Thiel and co-workers[29] show that the first channel (CIα) allows barrierless relaxation to S_0 in less than 150 fs through minimal rearrangement at C2, while the second, slower relaxation pathway requires a much greater structural distortion of both the C2 site and NH_2 amino group (CIβ). More recent simulations by Barbatti and co-workers[30] suggested that a $^1n\pi^*/S_0$ conical intersection (CIγ), involving out-of-plane distortion of the C6=O carbonyl group, may also play a minor role in the relaxation dynamics (≤ 5%).

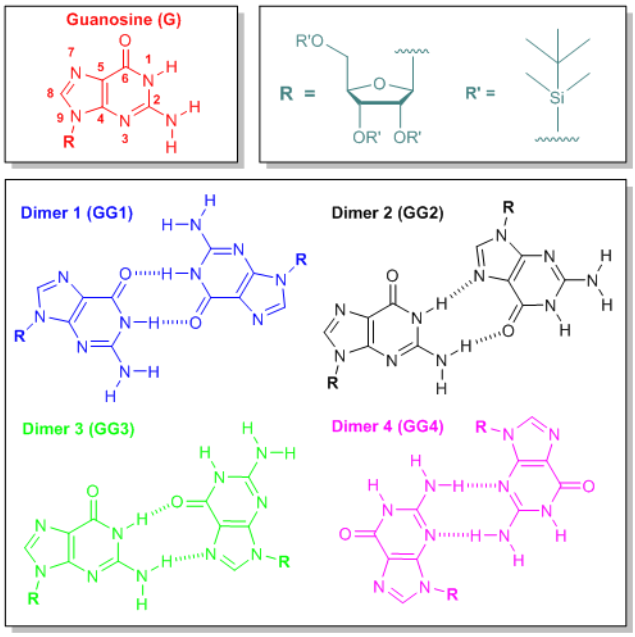

Fig. 1. Molecular structure and atom labels of guanosine (G, red), together with possible H-bonded GG dimer structures considered in this study. Structures of the ribose groups of the nucleoside (R) and the *t*-butyldimethylsilyl (R') protecting groups are shown in grey.

In nonpolar aprotic solvents, chemically modified derivatives of G have the capacity to form a variety of different self-assembled supramolecular aggregates. At concentrations of <1 M in apolar solvents (e.g. *n*-hexane), extended H-bonded 'ribbon' architectures of G have been shown to dominate, with some minor contribution from GG dimers and cyclic G_4 quartets.[31] Transient electronic absorption spectroscopy (TEAS) measurements by Hunger *et al*. on G ribbons in *n*-hexane at 267 nm led to the conclusion that, in competition with internal conversion to S_0, intersystem crossing populates a charge-separated triplet state

within 650 ps, which ultimately yields intermolecular EDPT.[32] However, similar experiments performed by Röttger *et al*. at 260 nm presented no evidence of EDPT or triplet state population for G aggregates in *n*-hexane and instead yielded a hierarchy of time constants, ranging from femtoseconds to nanoseconds.[31] These latter authors concluded that it was non-trivial to definitively assign individual time-constants to different aggregate sizes (dimers, ribbons etc.) within the complex mixture, although extensive H-bonding dramatically extends the excited state lifetime of G aggregates, relative to the G monomer. With respect to GG dimers though, more specific insight has previously been obtained through solvation of G derivatives in chloroform, which leads to a comparatively simpler mixture of dimers and monomers at sufficiently low concentrations (≤100 mM).[12,31] Although there is some debate over the specific dimer structures present in chloroform, fluorescence up-conversion experiments by Schwalb *et al*. were able to extract a fluorescence lifetime of 320 fs for GG dimers,[12] provisionally suggesting that, unlike G ribbons in *n*-hexane, dimerization leads to a shortening of the excited state lifetime compared to G monomers.

In the present study, we use an arsenal of spectroscopic techniques together with electronic structure calculations to resolve the electronic excited state relaxation dynamics of chemically modified GG homodimers and G monomers. All experiments are performed on silyl-protected G nucleosides in chloroform. A combination of density functional theory (DFT) and perturbation theory calculations, together with concentration dependent steady-state FTIR and two-dimensional infrared (2D-IR) spectroscopy, are first used to confirm that a mixture of monomers and dimers is present at ≤100 mM in chloroform, and that a single isomer dominates the dimer fraction (GG1, Fig. 1). Following excitation at 260 nm, the excited state relaxation dynamics are tracked using both TEAS and transient vibrational absorption spectroscopy (TVAS), which together reveal that GG homodimers have notably different relaxation dynamics than G monomers in chloroform. Insights from complementary electronic structure calculations suggest that: (i) monomer-like relaxation pathways are active in the GG dimers, albeit with modified dynamics because of subtle changes to the potential energy landscape in the vFC region from H-bonding; and (ii) the GG dimers may either be able to undergo EDPT, or access the lowest lying triplet (T_1) state.

2. Methods

2.1 Synthesis

To enable sufficient solubility of G in aprotic solvents, such as chloroform and *n*-hexane, the ribose O-H groups of the G nucleosides were protected by bulky, apolar *tert*-butyldimethylsilyl (TBDMS) groups (see Fig. 1). The synthesis of the protected 2',3',5'-tri-*O*-(*tert*-butyldimethylsilyl)-guanosine nucleosides (herein simply referred to as G) at the University of Kiel followed a modified protocol of Ogilvie.[33] The synthesis at the University of Bristol has also been described previously in detail.[11]

2.2 Two-dimensional Infrared Spectroscopy

2D spectra of the GG pairs were measured in a three-pulse photon echo experiment. Details of the experimental setup and the data processing and analysis have been described before.[34-37] In short, the mid-IR pulses were generated by a home-built parametric frequency converter driven by a 1 kHz regenerative amplified Ti- sapphire laser system. The output pulse was centred at the spectral region of interest. The resulting pulses had a spectral bandwidth >300 cm^{-1}, a pulse duration of 50 fs, and a pulse energy of 8 μJ. A diffractive optical setup was used to generate two pairs of phase-locked pulses of equal energy, three of which interacted with the sample in a photon echo sequence. Each pulse energy was about 600 nJ at the sample. The fourth pulse was attenuated and served as local oscillator to interfere with the generated nonlinear signal. Both the resulting nonlinear signal and local oscillator were dispersed by a monochromator providing the detection frequency ν_3. The resulting spectral interferograms were detected by an MCT detector array with a resolution of 8 cm^{-1}. The excitation frequency ν_1 was derived through analysis of the interferograms which were recorded as a function of the coherence time τ between pulse 1 and 2. 2D spectra were recorded for different waiting (population) times T_W between the second and the third pulse interacting with the sample.

Pump-probe experiments were performed using the same experimental setup, with two of the four pulses blocked. One pulse served as a pump, and the other pulse attenuated to 1% by a copper mesh served as a probe and was spectrally resolved and detected by an MCT detector. During the experiments, the sample solution was kept in a cell fitted with 100 μm PTFE spacers and BaF_2 windows of 1-mm thickness.

2.3 Transient Absorption Spectroscopy

TEAS experiments were performed at the University of Kiel, and the details of the apparatus have been presented elsewhere.[38,39] The transient absorption experiment was driven by the output of a Ti:Sapphire laser (ClarkMXR CPA 2001) which delivers pulses with pulse lengths of 150 fs (FWHM) at 775 nm. Half of the overall output of 1000 μJ/pulse was used for the transient absorption experiment. The excitation pulses were generated in a non-collinear optical parametric amplifier (NOPA) with subsequent temporal compression and frequency doubling. The resulting pulses had a center wavelength of 260 nm and a bandwidth of ~ 4 nm. For the generation of the broadband probe pulses, ~70 μJ/pulse of the laser fundamental was used. The laser pulses passed a delay stage (M-531.DG, Physik Instrumente) equipped with a retroreflector (CVI Melles Griot). They were attenuated to ~ 2 μJ by an absorptive neutral density filter and a combination of a λ/2 waveplate and a polarizer. These pulses were focused into a CaF_2 plate (d = 2 mm, Korth Kristalle) to produce a white-light continuum. The CaF_2 plate was rastered vertically and horizontally so that consecutive laser pulses hit different spots, thus ensuring that the low damage threshold of CaF_2 was not exceeded. The white light pulses were split into probe and reference beams using the front and back reflections from a planar glass plate. Pump and probe pulses were recollimated using reflective optics to reduce the chirp and obtain an optimal time resolution of the experiment. The pump pulses were set to magic angle polarization with respect to the probe pulses using a λ/2 waveplate. An optical chopper (MC2000, Thorlabs) equipped with a 10-shot blade (MC1F10, Thorlabs) was used to cut out every second laser pulse, thus enabling the measurement of background signals without excitation. The transmitted broadband light pulses were dispersed in a prism spectrograph and detected by two full-frame transfer back-thinned CCD cameras (Entwicklungsbüro Stresing, Berlin).

The protected G sample solutions were circulated through a home-built flow cell with two quartz windows (d = 0.2 mm, diameter 15 mm, Korth Kristalle) and a PTFE spacer of 100 μm thickness. A gear pump (Reglo-Z analog, Ismatec) equipped with an organic solvent resistant pumphead (Z-186 with PPS gears, Ismatech) and PTFE tubes was employed to flow the sample solution continuously through the cell. Transient absorption measurements for

each sample and the neat solvent were measured in one experimental run to avoid a change of coherent solvent signals. Each sample and solvent measurement was repeated three times to ensure reproducibility, and all measurements were repeated at least two times on different days with fresh sample solution. The purity and integrity of the samples were checked before and after each measurement via UV/vis absorption spectroscopy. The water content was reduced by preparing all sample solutions with anhydrous $CHCl_3$ in a flow box purged with dry air and checked before and after the transient absorption measurements via IR spectroscopy. TEAS measurements were performed with protected G sample concentrations of c_0 = 1.5 and 7.7 mM.

TVAS experiments were performed at the University of Bristol, using an apparatus that has been described in detail previously.[40] Briefly, the system consisted of a Coherent Vitara-S oscillator and Coherent Legend Elite HE+ regenerative amplifier, operating at 1 kHz and configured to produce 40 fs duration pulses at 800 nm with a total output power of 5 W. This fundamental beam was split into three parts using a series of beam splitters, only two of which were used for the current measurements and had energies of 2.45 mJ/pulse. These two beams seeded two Coherent OPerA Solo optical parametric amplifiers (OPAs). One of these OPAs produced spectrally tunable light spanning the UV to IR range (220 – 20,000 nm) and was used to generate the 260 nm (~100 fs) pump pulses for all the TVAS experiments reported here. The remaining OPA generated broadband (~300 cm^{-1}) tunable IR pulses for use as a probe in TVAS experiments, with energies of ~1 μJ/pulse at the sample.

For the TVAS measurements on G, the 260 nm pump pulse was attenuated to between ~0.6 and 1 μJ/pulse by cross-polarization using a λ/2 waveplate and wire-grid polarizer, and then focused ~2 cm behind the sample by a f = 200 mm CaF_2 lens. A beam profiler was used to determine a ~250 μm beam diameter for the Gaussian profile (full-width at half maximum) of the pump beam at the sample, returning pump fluences (F) in the range $F \approx 1.2 – 2$ mJ cm^{-2}. The polarization of the UV pump was maintained at the magic angle (54.7°), relative to the polarization of the IR probe pulse, by using the λ/2 waveplate in the UV pump beam line.

Broadband IR probe pulses were generated by difference frequency generation of the signal and idler beams from the IR OPA and for the experiments described here, were set to be centered at ~3400 cm^{-1} (N-H/O-H stretch region). The entire IR probe beam line was

enclosed by sealed plastic tubes and continuously purged by dry N_2 to avoid undesired absorption by atmospheric H_2O and CO_2. The IR probe pulses were reflectively focused into the sample to a tight ~50 μm beam diameter, so that the probed region of the sample was uniformly excited by the more loosely focused UV pump beam.

The temporal delay (*t*) between the UV pump and IR probe pulses was controlled by changing the path length of the pump beam with an aluminum retro-reflector mounted on a motorized delay stage, providing a maximum possible delay of t = 1.3 ns. The pump and probe beams then intersected the sample with a small crossing angle of ~5°. Prior to interaction with the sample, the UV pump beam was modulated at 500 Hz (blocking every other pulse) with an optical chopper wheel to obtain pump on/off spectra pairs at each *t*, which were then used to generate individual transient absorption spectra. After passing through the sample, the transmitted IR probe light was detected by a 128-pixel, liquid-N_2 cooled Mercury Cadmium Telluride array (Infrared Associates Inc., MCT-10-128) coupled to a spectrometer (HORIBA Scientific, iHR320), providing a spectral resolution of ~2 cm^{-1}.

Sample solutions of protected G (c_0 = 1 mM) were prepared in anhydrous $CDCl_3$ (Sigma-Aldrich, 99.99%). These sample solutions were then delivered through a stainless-steel flow cell, containing two 1.5 mm thick CaF_2 windows separated by a 380 μm thick Teflon spacer, which defined the absorption path length. The sample solution was flowed continuously through the cell by a peristaltic pump with PTFE tubing throughout.

2.4 Theoretical Calculations

A selection of *ab initio* and DFT calculations were used to assess the relative Boltzmann contributions of the four proposed GG dimers structures in chloroform (see Fig. 1). To make all calculations tractable (particularly with larger basis sets), methyl groups were used in place of the protected ribose groups (Fig. 1, R = CH_3). The relative ground state energies (without zero-point energy correction) of the GG dimers and the G monomer were calculated at the MP2 level of theory, together with its spin-component scaled counterpart (SCS-MP2). The SCS-MP2 method was selected for its acceptable description of energetics of non-covalent interactions (van der Waals and H-bonding) when benchmarked against both

experiment and higher level CCSD(T) calculations,[41,42] offering a computationally cheaper alternative to CCSD(T) calculations when the system is too large, such as the GG dimers. SCS-MP2 also provides an alternative to DFT methods, many of which (with the exception of functionals containing dispersion corrections[43]) commonly fail to capture dispersion interactions that can be key to obtaining reliable energetics of non-covalent interactions.[42,43] All MP2 level calculations were performed using the Gaussian 09 package[44] and the chloroform solvent was taken into account using a polarizable continuum model (PCM). Energies of ground state geometry optimized structures for G and the four GG dimers were obtained using the MP2 method, and the standard SCS energy correction factor to the second-order correlation correction was then obtained according to:

$$E^{\text{corr}}(\text{SCS-MP2}) = p_{\text{S}}E_{\uparrow\downarrow} + p_{\text{T}}E_{\uparrow\uparrow+\downarrow\downarrow}$$

where $E_{\uparrow\uparrow+\downarrow\downarrow}$ and $E_{\uparrow\downarrow}$ are the second-order perturbation contributions from double excitations of electron pairs with parallel and anti-parallel spins, respectively, and p_{S} = 6/5 and p_{T} = 1/3, according to Ref. [41]. All MP2 and SCS-MP2 calculations were performed with a Dunning cc-pVDZ basis set. Previous studies[42,45] have shown that larger triple-ζ and quadruple-ζ basis sets do not yield any significant improvement to the calculations.

Selected DFT calculations were also used to assess relative GG dimer energies and the nature of the vibrations in the N-H stretching region of the G monomer and all GG dimers. Ground state harmonic vibrational frequency calculations were performed on geometry optimized structures, all calculated at the PCM-PW91/6-311+G** level of theory using Gaussian 09. The PW91 functional[46] was selected for: (i) its reliable modeling of H-bonded nucleobase systems;[47,48] and (ii) its reasonable description of the relative frequencies and IR intensities of vibrations for G and GG structures, when benchmarked against steady-state FTIR and 2D-IR experiments (see Section 3.1). All calculated vibrations in the G monomer were scaled by 0.972, while H-bonded GG dimer vibrations were scaled by a factor of 0.960. Scaling factors were chosen to yield the best agreement with experimentally measured FTIR spectra. Other functionals were also trialled (M062X[49] and CAM-B3LYP[50]), as well as scaled harmonic frequencies using the MP2 method (*vide supra*), and found to yield qualitatively similar vibrational frequency results, although the scaled PW91 harmonic

frequencies were found to provide the best quantitative agreement with experimental observations.

Minimum energy conical intersection (MECI) geometries between the S_0 and S_1 states of the G monomer and GG1 dimer were located using a combination of seam model function (SMF),[51] single-component artificial force-induced reaction (SC-AFIR)[52] and spin-flip time-dependent density functional theory (SF-TDDFT).[53] The SF-TDDFT calculations were carried out using the GAMESS program[54] and the SMF/SC-AFIR approach using a developmental version of the Global Reaction Route Mapping (GRRM) program.[55] The SMF/SC-AFIR/SF-TDDFT searches were performed using the BHHLYP functional[56] and a 6-31G* basis set from the S_0 ground state equilibrium geometries. The model collision energy parameter for the SC-AFIR search was 100 kJ mol^{-1}.

Potential energy cuts (PECs) along the potential energy surface between the S_0 state minimum energy geometry and several low energy MECI geometries were constructed using the linearly interpolated internal coordinate (LIIC) methodology. Single point and vertical excitation energies, oscillator strengths and state characters for the singlet (S_n) or triplet (T_n) excited states of interest were calculated at the ADC(2)/def2-TZVP and ADC(2)/def2-SVP levels of theory for G and GG1, respectively, using TURBOMOLE.[57]

3. Experimental Results

3.1 Characterization of Monomer & Dimer Species

Previous literature has demonstrated that silyl-protected nucleosides have a strong propensity to undergo H-bonding dimerization upon solvation in chloroform.[12,58-60] In the case of silyl-protected G in chloroform, a comprehensive analysis of concentration dependent FTIR spectra in the N-H stretching region (3100 – 3600 cm^{-1}), such as those presented in Fig. 2a for c_0 = 1 and 10 mM, has been performed previously by Schwalb *et al*.[12] Analysis of spectra in the N-H stretching region was chosen over the carbonyl stretching region due to strong spectral overlap between monomer and dimer bands in the latter wavenumber range. The earlier analysis by Schwalb *et al*. returned a solvent dependent equilibrium constant for the dimerization of G monomers into H-bonded GG homodimers of $K_{GG} = [GG]/[G]^2 = 1010$

± 200 M^{-1}, where the error represents a value of 2σ. K_{GG} is related to the degree of association, β_{GG}, according to $K_{GG} = \beta_{GG}/2c_0(1-\beta_{GG})^2$, where $\beta_{GG} = 2[GG]/c_0$ and $c_0 = [G] + 2[GG]$ is the concentration of the G solution in chloroform. β_{GG} can thus be evaluated directly for a given c_0 value using the aforementioned value of K_{GG}. Table 1 summarizes β_{GG} fractions for c_0 concentrations used in the present study.

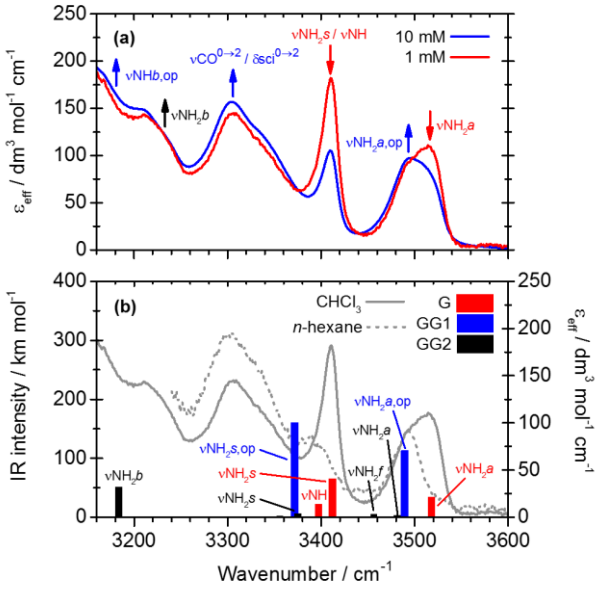

Fig. 2. (a) Concentration dependent FTIR spectra of G in chloroform at c_0 = 1 mM (red line) and 10 mM (blue line) in the N-H stretching region. Monomer and dimer bands are assigned according to the vibration labelling nomenclature for G (red), GG1 (blue) and GG2 (black) shown in Fig. 3 and assignments are based on calculated vibrational frequencies in panel (b). Band evolution with increasing concentration is indicated by the arrows. **(b)** Scaled harmonic vibrational frequencies (bars), calculated at the PCM-PW91/6-311+G** level (where R = CH_3, Fig. 1). Calculated IR band intensities of G, GG1 and GG2 have been scaled to simulate a 1 mM solution of G in chloroform (β_{GG} = 0.5) with the relative dimer contributions scaled according the calculated PCM-SCS-MP2/cc-pVDZ Boltzmann populations at 298 K - see Table 2. Harmonic frequencies are scaled by 0.972 for the monomer and 0.960 for dimers. FTIR spectra (grey lines) of G in chloroform (solid) and *n*-hexane (dashed) for c_0 = 1 mM are displayed for comparison.

For the concentrations used in the present study (≤100 mM), G solutions in chloroform are dominated by monomers and H-bonded dimers.[12,31] Neither extended H-bonded aggregation into ribbon structures, nor G_4 quartets (as seen in *n*-hexane solutions[31,32,60])

or π-stacking structures are found to contribute at our selected values of c_0.[12,60,61] However, consultation of earlier literature reveals that there is not a consensus regarding the exact structure(s) of the GG homodimers present in chloroform. Acknowledging earlier studies in both the gas- and solution-phases,[12,62] Röttger *et al*. depicted four possible structures for the GG dimer,[31] which are shown in Fig. 1. Earlier theoretical calculations on dimers of the simpler isolated guanine nucleobase suggested that the GG1 structure is by far the most stable of the isomers shown in Fig. 1.[62] Complementary gas-phase spectroscopy in this previous study returned no direct evidence for the presence of GG1 under molecular beam conditions, which was attributed to the fact that the optically bright $S_2 \leftarrow S_0$ transition was not excited in their hole burning experiments, due to a large exciton splitting shifting it out of their UV excitation window. Instead, so-called mixed dimer structures, containing both 7H and 9H tautomers of guanine, were identified as the dominant detectable species in the gas-phase, with no obvious evidence for GG2, GG3 or GG4 (when R = H).[62] For G nucleosides in chloroform, tautomerization into the 7H structure is prevented by addition of the ribose group in the N9 position (see Fig. 1). Consultation of FTIR spectra led Schwalb *et al*. to suggest that GG2 (often referred to as the reverse Hoogsteen structure) is the dominant isomer present in chloroform solution, rather than the symmetric GG1 structure;[12] GG3 and GG4 were excluded on energetic grounds. To investigate this issue further, and to enable interpretation of our subsequent TEAS and TVAS measurements, we revisit an analysis of FTIR spectra in the N-H stretching region (Fig. 2a), together with theoretical calculations on GG dimers (Table 2 and Fig. 2b) and complementary 2D-IR spectra to determine the GG dimer structure(s) present in chloroform solutions.

Fig. 2a presents FTIR spectra in the N-H stretching region for solutions of G in chloroform at both c_0 = 1 mM (red) and 10 mM (blue), corresponding to β_{GG} values of 0.5 and 0.8, respectively. Consistent with previous observations,[12,32] spectral bands located at 3410 cm^{-1} and 3520 cm^{-1} decrease in intensity with increasing concentration, and are assigned to the symmetric ($\nu NH_2 s$) and anti-symmetric ($\nu NH_2 a$) stretching modes of the NH_2 amino group of the G monomer. These modes are illustrated in Fig. 3. This assignment is verified by scaled harmonic vibrational frequency calculations at the PCM-PW91/6-311+G** level of theory on G (where R = CH_3), the results of which are shown by the red bars in Fig. 2b. These calculations also indicate that the low wavenumber edge of the 3410 cm^{-1} band

contains a contribution from the stretching mode of the secondary N-H amine group (νNH) of G, which has a calculated frequency of 3397 cm^{-1}.

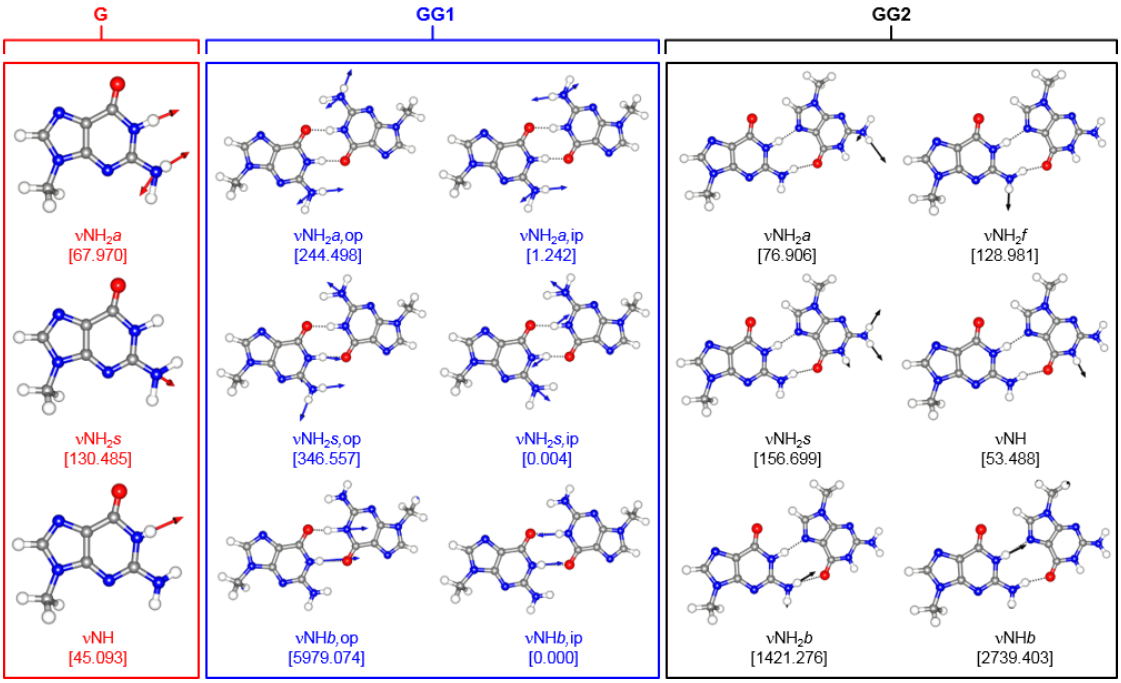

Fig. 3. Calculated vibrations and labels for G (red), GG1 (blue) and GG2 (black) at the PCM-PW91/6-311+G** level of theory, with R = CH_3. Unscaled calculated IR intensities (in km mol^{-1}) are given in square brackets. Additional labels for stretching motions of the primary amino (νNH_2) and secondary amine (νNH) groups are as follows: *a* = anti-symmetric stretch; *s* = symmetric stretch; op = out-of-phase coupled vibrations; ip = in-phase coupled vibrations; *b* = H-bonded group/bond; *f* = free N-H bond of an H-bonded amino group.

In addition to the reduction of G monomer bands, Fig. 2a also shows the growth of a broad, inhomogeneous feature peaking at 3310 cm^{-1} and the persistence of a sharper band at 3490 cm^{-1}. The latter feature is revealed as the νNH_2a band of the monomer declines with increasing concentration. Previously, Schwalb *et al*. assigned the features at 3310 and 3490 cm^{-1} to the 'bound' and 'free' N-H bonds of an H-bonded NH_2 group in the GG2 dimer[12] (labelled νNH_2b and νNH_2f, respectively, for GG2 in Fig. 3). In order to assess this assignment further and investigate the most likely structure(s) of the H-bonded GG dimers present in chloroform solution, MP2 and DFT calculations were performed to investigate

both the vibrational frequencies and relative energies of the four GG dimer structures in Fig. 1, where R = CH_3. Table 2 collates the calculated relative energies of the dimers (ΔE), the double H-bonding strength without zero-point energy correction (D_e) and the relative Boltzmann populations of the four dimers at 298 K (P_B) based on the values of ΔE for the given levels of theory. For all theoretical treatments used here, the symmetric GG1 dimer is found to be by far the most stable species, with D_e values ranging between 6919 cm^{-1} (MP2) and 5963 cm^{-1} (PW91), and a P_B fraction in excess of 92 % in all cases. The reverse Hoogsteen structure, GG2, previously proposed to dominate the GG dimer fraction in chloroform,[12] is found to be between 529 cm^{-1} (SCS-MP2) and 1035 cm^{-1} (PW91) less stable than GG1 in chloroform, with a maximum calculated P_B of 7.2 %, as returned by PCM-SCS-MP2/cc-pVDZ. The remaining GG3 and GG4 structures were found to be >1300 cm^{-1} less stable than GG1, in both cases, and as previously suggested have a negligible contribution to the dimer fraction in chloroform (≤0.2 %) [12].

We benchmarked our calculations against FTIR measurements, with Fig. 2b presenting simulated IR transition strengths (in km mol^{-1}) for a 1:1 ratio of H-bonded GG dimers (blue & black bars) and G monomers (red bars), corresponding to a c_0 = 1 mM solution of G in chloroform (β_{GG} = 0.5). The calculated IR transition strengths for the modes of all four GG dimers (at the PCM-PW91/6-311+G** level of theory) were scaled according to the P_B fractions returned by PCM-SCS-MP2/cc-pVDZ, in order to highlight our calculated upper limit for contributions from GG2 (black bars) to the FTIR spectrum, relative to GG1 (blue bars). Harmonic frequencies were scaled by factors of 0.972 and 0.960 for G and GG species, respectively. It is immediately clear that this simulated spectrum is dominated by bands from GG1 and G monomers, with only a minor contribution from GG2 at 3183 cm^{-1}. Comparison of this simulated mixture to the c_0 = 1 mM FTIR spectrum of G in chloroform (Fig. 2b, solid grey line) shows good agreement between the calculated and experimentally observed locations of the G monomer modes, as well as a calculated mode of the GG1 dimer at 3489 cm^{-1} and the sharp dimer band at 3490 cm^{-1}. Although localized normal mode interpretations of vibrations in H-bonded systems should be treated with caution,[63] our calculations indicate that the feature at 3490 cm^{-1} can plausibly be assigned to a coupled vibration in GG1, where the anti-symmetric NH_2 stretch motions of the two G units vibrate out-of-phase with respect to each other, labeled νNH_2a,op in Fig. 3. An analogous out-of-phase coupled

vibration, with a similar IR transition intensity to νNH_2a,op, is also calculated for the symmetric NH_2 stretch motions in GG1 at 3372 cm^{-1} (νNH_2s,op, Fig. 3); the in-phase counterparts to these two modes possess negligible IR transition strengths (νNH_2s,ip and νNH_2a,ip, Fig. 3). Despite this, it is not immediately clear that a band associated with νNH_2s,op is present around 3370 cm^{-1} in the FTIR spectrum. In principle, it is tempting to assign the broad inhomogeneous feature peaked at 3310 cm^{-1} to νNH_2s,op of GG1. However, conventional wisdom would suggest that the νNH_2s,op band should be a relatively narrow feature, similar to the lineshape of νNH_2a,op at 3490 cm^{-1}, given that neither mode will experience any substantial inhomogeneous broadening as a result of G to G H-bonding and the relatively weak interaction with the chloroform solvent. Based on the broad, inhomogenous lineshape of the 3310 cm^{-1} feature, we discount its assignment to νNH_2s,op of GG1, and return to discuss the identity of this feature later. Instead, we propose that, in chloroform solution, the νNH_2s,op mode of GG1 is present around 3370 cm^{-1}, but remains hidden by both the adjacent 3310 cm^{-1} band and νNH_2s band of the G monomer.

To test our assumption that νNH_2s,op of GG1 is present in the FTIR spectrum of G in chloroform, but remains obscured, additional experiments have been performed. Figure 2b also reports the FTIR spectrum of G in *n*-hexane at c_0 = 1 mM (dashed grey line), where only dimers and higher-order H-bonded aggregates of G are present.[31,32] Unlike the analogous FTIR spectrum in chloroform, the monomer features are absent from the spectrum of G in *n*-hexane, fully resolving a sharp feature at 3490 cm^{-1} belonging to νNH_2a,op of GG1 (and/or a related vibration in higher-order G ribbons containing the GG1 motif – see Fig. 1 in Ref. [31]) together with the broad 3310 cm^{-1} band. A narrow shoulder on the high wavenumber edge of the 3310 cm^{-1} band is also revealed in *n*-hexane, centered around 3380 – 3390 cm^{-1}. We propose that this new feature belongs (in part) to the predicted νNH_2s,op mode of GG1, but acknowledge that contributions from extended G aggregates cannot be excluded.

Further insight is gained through 2D-IR experiments, which have been performed as an analytical tool. An absorptive 2D-IR spectrum of a 100 mM G solution in chloroform (β_{GG} = 0.93) in the N-H stretching region is presented in Fig. 4, for a waiting time of T_W = 100 fs. The spectrum is reminiscent of 2D-IR spectra reported for other H-bonded DNA nucleosides in chloroform at similar T_W.[58,59] A waiting time of T_W = 100 fs has been selected so that

the effects of both intermolecular and intramolecular vibrational energy redistribution are minimized, which will dominate at later T_W. The diagonal of the 2D-IR spectrum is comparable to the linear FTIR spectrum (Fig. 4, upper panel), containing similar features and relative intensities. Cross peaks between features on the diagonal indicate that they belong to different vibrational modes of a common species, aiding in: (i) our confidence of assignment to multiple species in the linear FTIR spectrum and; (ii) identification of peaks in the linear spectrum that are obscured by overlapping bands, such as νNH_2s,op of GG1. A strong cross peak (region i) is identified between νNH_2a,op at 3490 cm^{-1} and the broad feature at 3310 cm^{-1} (the latter of which is deliberately presented saturated along the diagonal of Fig. 4), confirming that the 3310 cm^{-1} band indeed belongs to GG1. In the area labeled ii, this cross peak extends to higher wavenumber along the excitation frequency axis, which we cautiously suggest is a non-zero coupling between νNH_2a,op at 3490 cm^{-1} and νNH_2s,op at 3390 cm^{-1} of GG1; such a cross peak cannot arise from a coupling between νNH_2s of G and νNH_2a,op of GG1. Taken in isolation, we acknowledge that such an assignment would be tenuous, given the weak intensity of the cross peak in region ii, the spectral congestion in the N-H stretching window and the spectral resolution available in our 2D-IR measurements. However, our confidence in this assignment is arrived at by taking our 2D-IR observations together with our theoretical frequency calculations, the complementary findings from FTIR spectra of G in *n*-hexane and NMR spectroscopy. The analysis of NMR spectra finds no evidence for the presence of an asymmetric dimer, and is fully consistent with GG1 being the dominant dimer in chloroform solution (Fig. S1 of Supporting Information).

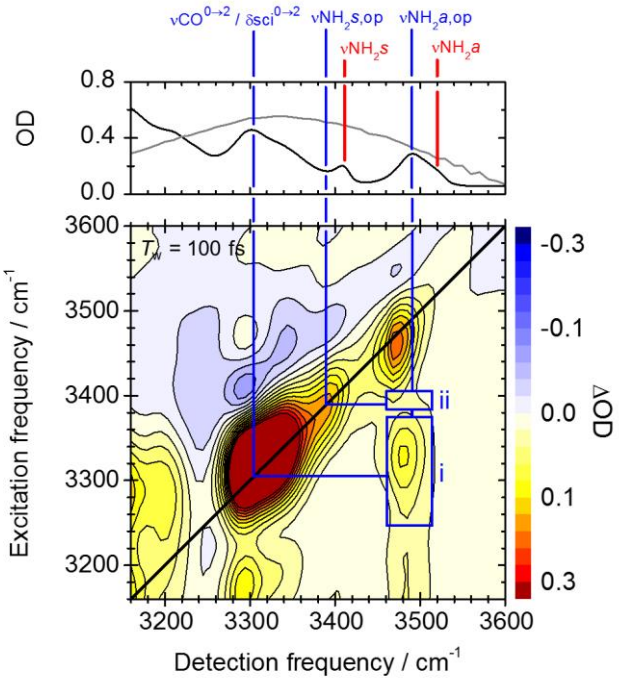

Fig. 4. Absorptive 2D-IR spectrum of c_0 = 100 mM G in chloroform (G = 7 %, GG = 93 %) in the N-H stretching region for a waiting time of T_w = 100 fs. The spectrum was recorded for excitation and local oscillators in a parallel polarization geometry. The spectrum is plotted on a 'saturated' scale to reveal additional information about mode couplings, examples of which are identified in regions i and ii. A linear FTIR spectrum for a c_0 = 100 mM G solution in chloroform is given above for reference (black line), including the spectral profile of the IR excitation/detection pulse (grey line). See Fig. 3 for mode label information.

The identity of the broad 3310 cm^{-1} feature belonging to GG1 merits further discussion. Based on our frequency calculations, one possible assignment is to an out-of-phase coupled stretching vibration of the two H-bonded secondary N-H amine groups (ν*NHb*,op in Fig. 3). A similar assignment for this feature has been made previously, albeit for a H-bonded mode of the GG2 dimer.[12,31,32] However, our scaled harmonic frequency calculations predict this mode at a significantly lower wavenumber of 2804 cm^{-1} with a calculated IR intensity that is an order of magnitude stronger than either νNH_2*a*,op or νNH_2*s*,op (5979 km mol^{-1}, see Fig. S2). This prediction is more consistent with a very strong, broad band observed around 3100 cm^{-1} in the FTIR spectrum of G in chloroform, which we do not present in full in Fig. 2a, as this feature is convolved with a comb of intense, narrow bands belonging to the TBDMS protecting groups (see Fig. 1 in Ref. [37]). The high wavenumber edge of this

feature can be seen between 3160 and 3240 cm^{-1} in Fig. 2a, and is labelled accordingly; we speculate that the small shoulder at 3210 cm^{-1} may belong to the νNH_2b mode of the minor GG2 isomer. Given these observations, the most plausible assignment for the 3310 cm^{-1} band is a Fermi resonance of the v = 2 ← v = 0 transition of the carbonyl stretching mode ($\nu CO^{0\rightarrow 2}$) with the strong, inhomogenously broadened νNHb,op mode of GG1. An analogous assignment was made for a similar feature at 3300 cm^{-1} in the FTIR spectrum of GC Watson-Crick base pairs in chloroform,[12] while Nibbering and co-workers showed that intermolecular H-bonding has a propensity for enhancing Fermi resonances.[63,64]

3.2 Transient Absorption Spectroscopy of Guanosine in Chloroform

Ultrafast transient electronic and vibrational absorption spectroscopies have been used to examine G monomers and GG1 dimers in chloroform, and to compare the excited state relaxation dynamics and subsequent recovery of the S_0 ground state following UV photoexcitation. In both cases, excitation at 260 nm (4.77 eV) populates optically bright $^1\pi\pi^*$ states, formed through a $\pi^* \leftarrow \pi$ transition (see Fig. 5). For G, previous studies on the guanine nucleobase [24,26,28-30] and our present calculations on 9-methyl-guanine indicate that two possible $^1\pi\pi^*$ states can be excited, and are labeled ^1L_a and ^1L_b in Platt notation[65] (S_1 and S_3, respectively, in Table 3), from which a variety of electronic state couplings offer competing relaxation pathways to recover S_0 molecules.[24-26,28-30] Our calculations also suggest that two bright $^1\pi\pi^*$ states are accessible around 260 nm in GG1 (S_2 and S_3 in Table 3). Both states involve occupation of π and π^* orbitals that are fully delocalized across the entire GG1 dimer in the vFC region (necessitated by C_{2h} symmetry). This is in contrast to π systems in heterodimers, such as the GC Watson-Crick base pairs,[66] where the π orbitals remain localized on an individual moiety within the dimer, giving rise to $^1\pi\pi^*$ states with either locally excited or charge-transfer character in the vFC region. To the best of our knowledge, the present literature has not explored the possible excited state relaxation pathways available to the GG1 dimer, which we return to discuss in Section 4.2.

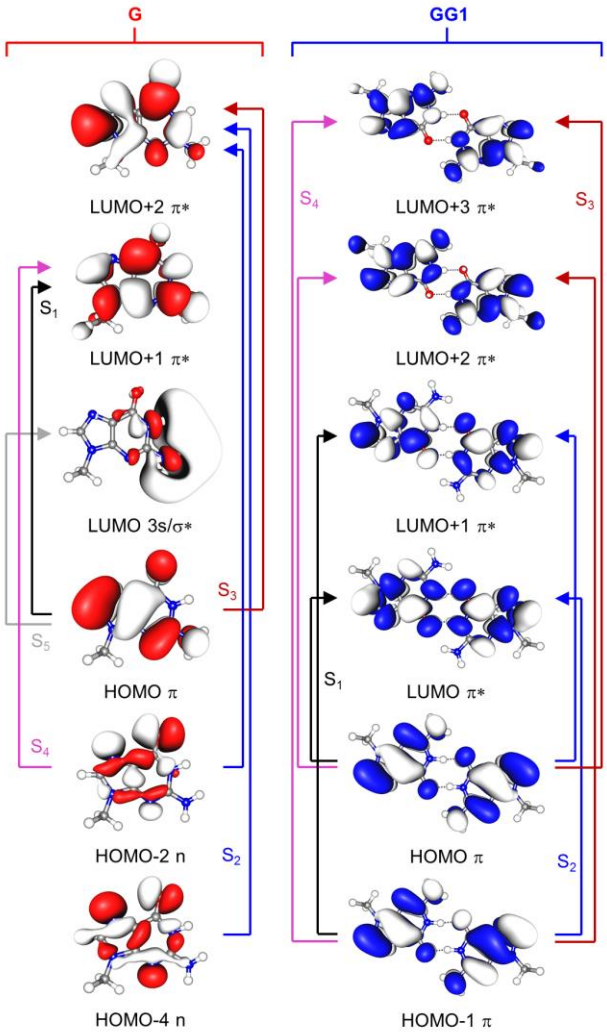

Fig. 5. Dominant orbital transitions involved in the singlet excited states (S_n) of G (left) and GG1 (right), calculated at the PCM-ADC(2)/def2-TZVP and PCM-ADC(2)/def2-SVP levels of theory, respectively. Table 3 summarizes the transition contributions to a given state.

Fig. 6a displays an example TEA spectrum, presented as a 2-D false color intensity map, recorded following 260-nm photoexcitation of a 1.5 mM G solution in $CHCl_3$ (G = 43%, GG = 57%). Immediately after t = 0, the spectrum is dominated by a broad positive transient absorption signal, which we assign to excited state absorption (ESA). The ESA signal spans the entire UV/visible probe wavelength range ($330 < \lambda_{probe} < 720$ nm) and steadily increases in intensity towards shorter UV wavelengths. No obvious time dependent spectral shifts or structure are observed in the ESA profile as it decays over time. At $\lambda_{probe} > 500$ nm the ESA

signal almost entirely decays within the first 1 ps, signalling that some fraction of the photo-excited G and GG1 mixture in $CHCl_3$ undergoes ultrafast relaxation back to its S_0 ground state, consistent with previous expectations for the G monomer.[12,21-23] However, it is clear that ESA decay at $\lambda_{probe} < 400$ nm instead occurs over a timeframe of picoseconds, also indicating that a portion of this excited ensemble relaxes more slowly.

A quantitative analysis of the ESA decay kinetics recorded in the TEA spectrum was performed by simultaneously fitting time dependent intensity profiles at 8 different λ_{probe} values. Two examples of these fitted ESA decay profiles are presented in Fig. 6b and 6c for λ_{probe} values of 340 nm and 560 nm, respectively. The fitting process required a minimum of three exponential decay functions to model accurately all 8 different λ_{probe} datasets, returning time-constants of: $\tau_2 = 210 \pm 20$ fs, $\tau_3 = 2.6 \pm 0.1$ ps and $\tau_4 = 18 \pm 2$ ps. These τ_n values and their associated fit amplitudes (A_n) for a given λ_{probe} are collated in Table 4. Although we broadly attribute these time-constants to excited state decay processes, at this stage the TEAS measurements alone do not make it possible to discern whether these τ_n values belong to either G, GG1 or a combination of both species. We note though, that τ_2 and τ_3 are reminiscent of lifetimes obtained for the G monomer in $CHCl_3$ from fluorescence up-conversion studies at 262 nm.[12] We return to consider the identity of these time-constants below when we analyze data obtained from TVAS.

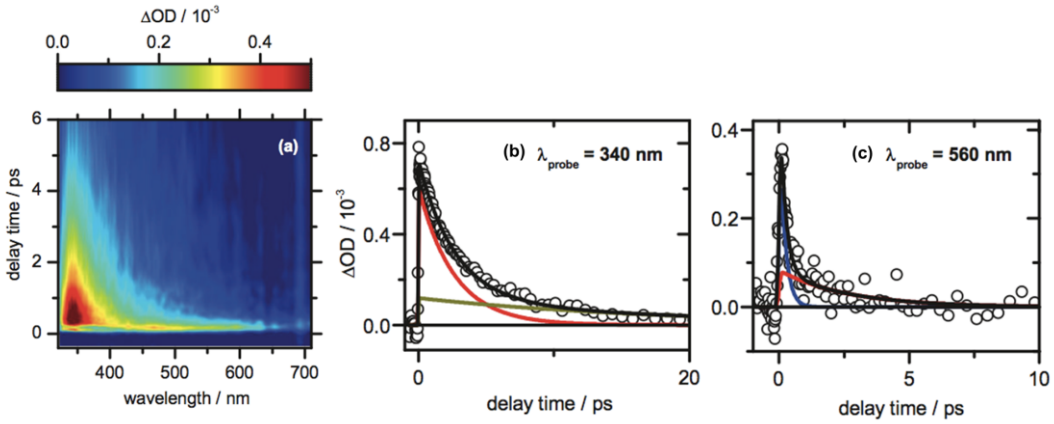

Fig. 6. (a) Two-dimensional false color intensity map of the TEA spectrum obtained from G in $CHCl_3$ ($c_0 = 1.5$ mM, G = 43%, GG = 57%) following excitation at 260 nm. Absorption change profiles as a function of delay time obtained from (a) at probe wavelengths of **(b)** $\lambda_{probe} = 340$ nm and **(c)** $\lambda_{probe} = 560$ nm. Open circles = experimental data, black line = total fit. Colored lines are decay components

with time constants of τ_2 = 210 fs (blue line), τ_3 = 2.6 ps (red line) and τ_4 = 18 ps (green line). See Table 4 for the fit amplitudes (A_n) associated with each τ_n component.

Table 4 also includes a time-constant of τ_1 = 70 ± 10 fs. τ_1 emerges when kinetic fits are performed on time dependent intensity profiles extracted from a TEA spectrum recorded after 260-nm excitation of a 7.7 mM G solution in $CHCl_3$ (G = 22%, GG = 78%), rather than a c_0 = 1.5 mM sample. The τ_1 value obtained from measurements on the c_0 = 7.7 mM solution only contributes at UV probe wavelengths (λ_{probe} = 340 nm) and possesses a negative fit amplitude. We assign τ_1 to decay of stimulated emission signal as the excited state wavepacket evolves from the νFC region on the $^1\pi\pi^*$ state, which is only clearly resolved at higher concentrations due to improved signal-to-noise. In principle, τ_1 can be included in the analysis of the λ_{probe} = 340 nm decay trace at c_0 = 1.5 mM, although it is not necessary to produce an adequate fit. Once again, we cannot yet state which specific species τ_1 is associated with, although its prominence at higher c_0 may hint it arises from GG1.

TVA spectra recorded in the N-H stretching region (3360 – 3640 cm^{-1}) provide complementary insights into the timescales for excited state relaxation/ground state recovery, subsequent cooling dynamics of nascent vibrationally hot S_0 molecules and the formation of any photoproducts. Fig. 7a presents a TVA spectrum recorded following 260-nm photoexcitation of a 1 mM solution of G in $CDCl_3$ (G = 50 %, GG = 50%). At the earliest presented delay time of t = 1 ps, several negative changes in optical density (ΔOD) are observed, henceforth termed ground state bleach (GSB) features, which reflect population transfer from S_0 into electronically excited state molecules through UV absorption. Based on our characterization of FTIR spectra in Section 3.1, spectrally resolved GSB features at 3310 and 3410 cm^{-1} can be assigned to the $\nu CO^{0\rightarrow2}/\delta sci^{0\rightarrow2}$ Fermi resonance of GG1 and the νNH_2s stretching mode of G, respectively, while the νNH_2a,op and νNH_2a modes of GG1 and G both contribute to the GSB band at ~3510 cm^{-1}. Cursory inspection of Fig. 7a indicates that all GSB features reduce in depth over time, although their specific recovery timescales vary. Similarly, the residual GSB signal remaining at the maximum temporal delay of our experiments (t = 1.3 ns) varies: the νNH_2s GSB recovers completely, whereas ~15% of the initial $\nu CO^{0\rightarrow2}/\delta sci^{0\rightarrow2}$ GSB amplitude persists, already hinting at different excited state dynamics/photochemistry for G and GG1. Within the first 15 ps, positive ΔOD features are

also observed on the low wavenumber edges of the GSB features, which blue-shift and decay over time. The most prominent of these positive bands is observed at 3460 cm^{-1} and labeled ν*NH in Fig. 7a. Such features are characteristic of vibrationally hot S_0 species formed following ultrafast internal conversion of electronically excited molecules, which then cool through vibrational energy transfer to the surrounding solvent.[11,67]

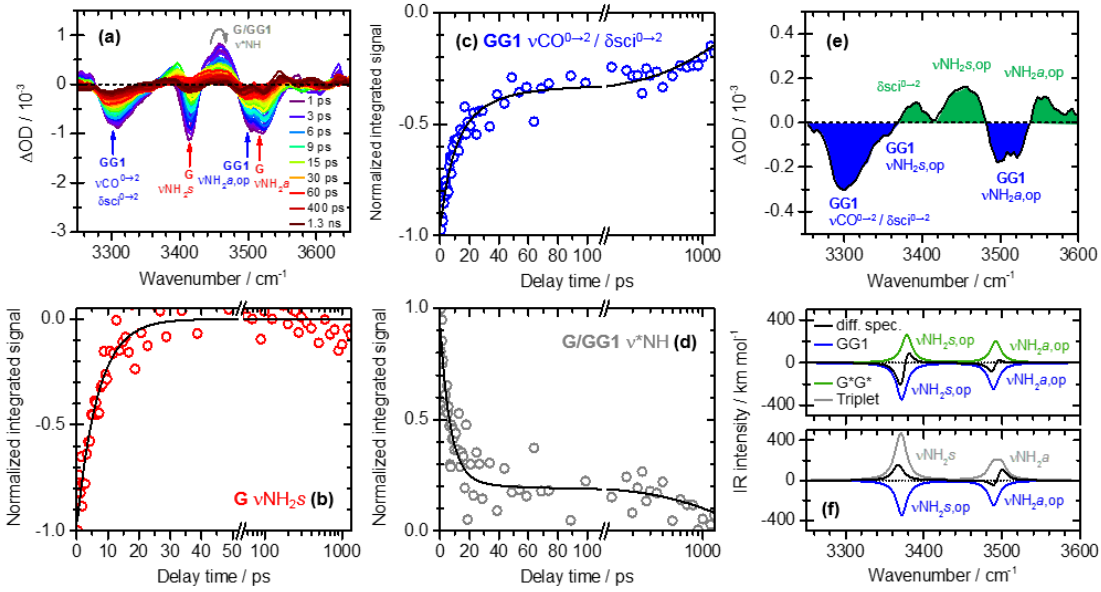

Fig. 7. (a) TVA spectra recorded for G in $CDCl_3$ (c_0 = 1 mM) following excitation at 260 nm and probing in the N-H stretching region (3250 - 3650 cm^{-1}) (G = 50%, GG = 50%). Normalized integrated signal traces (open circles) and kinetic fits (black lines) as a function of delay time for **(b)** the symmetric NH_2 stretch bleach (νNH_2*s*, 3415 cm^{-1}) of the monomer, **(c)** the v = 2 ← v = 0 Fermi resonance bleach ($\nu CO^{0\rightarrow2}$ / $\delta sci^{0\rightarrow2}$, 3310 cm^{-1}) of the dimer, and **(d)** vibrationally hot N-H stretch ground state (ν*NH, 3460 cm^{-1}) of both the monomer and dimer. ν*NH also contains contributions from the decay of dimer photoproduct molecules – see main text for details. See Table 4 for details of τ_n fit amplitudes (A_n). **(e)** Decay associated spectrum for the τ_6 = 1.4 ns component of the kinetic fits, extracted from a global fitting analysis of the TVA spectra in (a) using Glotaran. **(f)** Calculated difference spectra between GG1 and G*G* tautomer (upper panel) and GG1 and GG1 T_1 triplet state (lower panel). Scaled harmonic frequencies calculated at the PCM-PW91/6-311+G** level, where R = CH_3 (see Fig. 1).

By performing TVAS in the N-H stretching region, the ground state recovery dynamics of the G monomer and GG1 dimer can be readily resolved by integrating GSB features associated with only a single species and independently analyzing the respective recovery kinetics. Such

an analysis is not feasible with TEAS, or TVAS in the carbonyl stretching region, where ESA or GSB features for G and GG1 are spectrally overlapped. In particular, the νNH_2s and $\nu CO^{0\rightarrow2}/\delta sci^{0\rightarrow2}$ bands in Fig. 7a prove to be ideal reporters for G and GG1 dynamics, respectively; the convoluted nature of the GSB at ~3510 cm^{-1} means we do not analyze this feature further. Integration of the νNH_2s and $\nu CO^{0\rightarrow2}/\delta sci^{0\rightarrow2}$ GSB features over 10 cm^{-1} wide intervals about their band centers returns the time dependent intensity profiles in panels b and c of Fig. 7, respectively. Analogous treatment of the ν*NH hot band, which contains contributions from both G and GG1, yields the decay trace in Fig. 7d. All three kinetic traces share an initial rapid recovery, although in contrast to the G monomer (νNH_2s, 3410 cm^{-1}, panel b), it can be seen that the GG1 dimer ($\nu CO^{0\rightarrow2}/\delta sci^{0\rightarrow2}$, 3310 cm^{-1}, panel c) and the G/GG1 hot band (ν*NH, 3460 cm^{-1}, panel d) also possess a significant fraction of signal that recovers much more slowly. Given the element of common recovery dynamics in all three time-dependent traces, the kinetic traces are globally fitted using a single set of exponential decay functions, returning one set of time-constants. The time-constants (τ_n) and the associated amplitudes (A_n) returned from this global kinetic analysis are presented in Table 4, together with τ_n and A_n values obtained from TEAS.

Complete recovery of the νNH_2s GSB associated with the G monomer is well described by a single exponential decay function with a time-constant of τ_5 = 6.7 ± 0.5 ps. Approximately 73% of the ν*NH hot band decay can also be modelled with τ_5 as well, indicating that this time-constant is related to cooling of electronically S_0 but vibrationally hot G molecules. The presence of ν*NH at our earliest recorded time delay (t = 1 ps) indicates that at least some fraction of the photo-excited G ensemble possesses a sub-picosecond excited state lifetime, giving rise to ultrafast formation of vibrationally hot S_0 molecules through internal conversion. This conclusion agrees with the τ_2 = 210 ± 20 fs time-constant extracted from our TEAS measurements, leading us to suggest that (at least some component of) τ_2 corresponds to the lifetime of G monomers in their $^1\pi\pi^*$ (L_a/L_b) state(s). This suggestion is in accord with the 430-fs lifetime deduced from previous fluorescence up-conversion measurements by Schwalb *et al*. [12] for a 262-nm excitation wavelength. These authors also reported that a portion of UV-excited G monomers relaxes with a slower time-constant of 4.2 ps at 262 nm, which is similar to our τ_3 = 2.6 ± 0.1 ps value obtained from TEAS at 260 nm. As such, we

also assign τ_3 to relaxation of excited G molecules and propose that relaxation occurs *via* two different channels following bifurcation of excited state flux in the νFC region. We return to discuss the identities of these two pathways in Section 4.1. Given that both τ_2 and τ_3 are more rapid than the timescale for vibrational cooling of G in S_0, the νNH_2s GSB recovery kinetics are dictated by the rate-limiting τ_5 value of 6.7 ps. Based on previous literature,[40,68] the 6.7 ps time-constant most likely corresponds to the final v = 1 → v = 0 step of the vibrational cooling ladder in S_0, with similar cooling rates observed for pyrimidine nucleosides and GC Watson-Crick base pairs in chloroform.[11,67]

From kinetic fits to the $\nu CO^{0\rightarrow2}/\delta sci^{0\rightarrow2}$ GSB presented in Fig. 7c, Table 4 shows that the initial rapid recovery of S_0 (v = 0) ground state population for the GG1 dimer can also be modelled with τ_5 = 6.7 ps (28%). Given that the G monomer does not contribute to the $\nu CO^{0\rightarrow2}/\delta sci^{0\rightarrow2}$ GSB feature, this indicates that both the monomer and dimer experience very similar solute-solvent coupling during vibrational energy transfer to the $CDCl_3$ bath – a similar observation has been made for the imino-oxo and amino-oxo tautomers of cytidine in chloroform.[67] It also implies that ~30% of the photo-excited GG1 ensemble undergoes ultrafast relaxation back to S_0, in-line with the previously reported 320-fs fluorescence lifetime for GG dimers.[12] In our present measurements, we therefore suggest that some portion of the τ_2 = 210-fs value extracted from TEAS may be associated with decay of excited GG1 dimers.

After the initial recovery described by τ_5, our kinetic analysis indicates that two additional time-constants, with values of τ_4' = 19 ± 5 ps (36%) and τ_6 = 1.4 ± 0.6 ns (36%), are required to adequately model the remaining ~70% of the $\nu CO^{0\rightarrow2}/\delta sci^{0\rightarrow2}$ GSB recovery. Within the returned error bars $\tau_4' \approx \tau_4$ = 18 ps, implying that they both describe the same photo-physical process. As τ_4 is only associated with recovery of the $\nu CO^{0\rightarrow2}/\delta sci^{0\rightarrow2}$ GSB in TVAS, we conclude this process is exclusive to the relaxation dynamics of photo-excited GG1 dimers. Possible assignments for this dimer-only pathway include monomer-like relaxation, where the dynamics have been modified through the effects of H-bonding, or EDPT, which is only feasible in the H-bonded dimer. Both of these pathways have been observed previously for related systems,[6,11] and we discuss these processes further in Section 4.2. It merits note that in earlier fluorescence up-conversion studies on GG dimers, no signal was observed over

an extended picosecond timeframe,[12] indicating that the state/pathway associated with τ_4 must be optically dark to fluorescence at 350 nm.

The final recovery component of τ_6 = 1.4 ns for the $\nu CO^{0\rightarrow2}/\delta sci^{0\rightarrow2}$ GSB is two-orders of magnitude slower than τ_4, accounting for ~35% of the observed GG1 dynamics. Kinetic fits to the ν*NH hot band also indicate that τ_6 describes 23% of the positive ΔOD signal decay at 3460 cm^{-1} (the final 4% of ν*NH decay is modelled by τ_4). Although τ_6 contributes to the decay kinetics of the integrated ν*NH hot band, for molecular systems of this size in chloroform, a time-constant of 1.4 ns is unlikely to describe an additional slower vibrational cooling process in the S_0 state of GG1 (*cf.* τ_5 = 6.7 ps). Instead, we propose that τ_6 describes the decay of an intermediate state/photoproduct of GG1 with a vibrational band located around 3460 cm^{-1}, which is initially masked by ν*NH in our TVA spectra at $t < 10$ ps.

In order to obtain an insight into the difference-spectrum profile of the intermediate/photoproduct, we extracted the decay associated spectrum (DAS) for the τ_6 component of our fits by performing a global target analysis of the TVA spectra in Glotaran.[69] Although DAS obtained from TVAS are open to misinterpretation, an analysis of TVA spectra at time-delays after the vibrational cooling dynamics have subsided (*i.e.* when major spectral shifts are complete, *cf.* the ν*NH hot band) can in principle provide useful information,[70] as is the case here for τ_6. Fig. 7e presents the DAS for the τ_6 = 1.4 ns component of our fits, confirming that only the GSB features at 3310 cm^{-1} ($\nu CO^{0\rightarrow2}/\delta sci^{0\rightarrow2}$) and ~3500 cm^{-1} (νNH_2a,op) associated with the GG1 dimer contain a τ_6 recovery component (blue shading). τ_6 has a fit amplitude of zero at the location of the G monomer νNH_2s GSB (3410 cm^{-1}). The DAS also reveals three new vibrational markers peaked at approximately 3390 cm^{-1}, 3450 cm^{-1} and 3550 cm^{-1} (green shading), implying that the intermediate/photoproduct species possesses vibrational modes that are blue-shifted relative to GG1.

Two plausible assignments for τ_6 are proposed here. The first is slow decay of a double H-atom transferred tautomer (henceforth G*G*), formed through an ultrafast (quasi-) concerted double EDPT mechanism. Photoproduct formation through a double H-atom transfer process has recently been confirmed for GC Watson-Crick base pairs in chloroform[11] and

theoretically investigated for related homodimer species.[71] In the case of G*G*, slow decay of the tautomeric photoproduct back to GG1 could be envisaged *via* H-atom tunneling on S_0 through a small energy barrier.[72] Alternatively, τ_6 may arise from decay of population trapped in triplet states. For extended H-bonded G ribbons in *n*-hexane, triplet state population has been posited as a possible slow decay route.[32] Fig. 7f shows simulated difference-spectra, generated from the results of scaled harmonic vibrational frequency calculations at the PCM-PW91/6-311+G** level, for a G*G* tautomer (green, upper panel) and the T_1 ($^3\pi\pi^*$) state of GG1 (grey, lower panel). In both scenarios, these simulations imply that there should be a small blue shift of the photoproduct frequency relative to the νNH_2a,op GSB of GG1 around 3500 cm^{-1}, consistent with our extracted DAS for τ_6 in Fig. 7e. However, agreement between the DAS and either of the simulated spectra below 3500 cm^{-1} is not as clear-cut. We return to consider these possible assignments for τ_6 in Section 4.2.

4. Discussion

In order to investigate possible deactivation pathways, and to attempt to understand the discrepancies in the time constants observed experimentally for the G monomer and dimer, we performed a full MECI search using the GRRM program [51,52,55] and investigated a variety of potential relaxation pathways using interpolation methods. The results of static calculations presented here cannot be used to predict lifetimes directly, but they provide some indication of the likelihood of certain deactivation mechanisms. The mechanisms and timescales discussed in this section for G monomers and GG1 dimers are summarized in Table 4.

4.1 Monomer Relaxation Pathways

For the isolated guanine monomer, previous dynamics calculations of the energetic deactivation pathways indicate that passage through two S_1/S_0 conical interactions (here labelled CIα and CIβ) is responsible for driving the majority of population transfer to the electronic ground state.[29,30] The previously reported geometry of CIα involves pyramidalization at the C2/NH_2 site (see Fig. 1 for atom labelling), whereas CIβ involves a smaller out-of-plane distortion of C2 and a significant distortion of the NH_2 group, resulting

in it being nearly perpendicular to the molecular plane. The MECI geometries reported in this work (from SF-TDDFT calculations) for 9-methyl-guanine are nearly identical to the previously reported structures for guanine, although for CIα, there is a rotation of the NH_2 group.

Interpolated pathways from the Franck-Condon region to the three lowest energy conical intersections located with the GRRM search (CIα, CIβ, CIγ, Fig. 8) indicate no energetic barriers *en route* to any of the CIs. However, the PES for approach to CIγ, which is predominantly ππ* in character, is significantly flatter on exiting the vFC region than for the other two CIs. Branching between these competing pathways cannot be predicted from the energetics calculations alone, but previous work from Thiel and co-workers suggests that passage via CIα is the dominant relaxation pathway, with a smaller contribution (~40 %) via CIβ because of the larger geometric distortion required to reach the CIβ structure.[29] The computed time constants for these pathways (190 fs and 400 fs) and the relative branching ratios are supported by further dynamics simulations by Barbatti et *al.*[30], with the addendum that passage via CIγ may account for approximately 5 % of the population transfer.

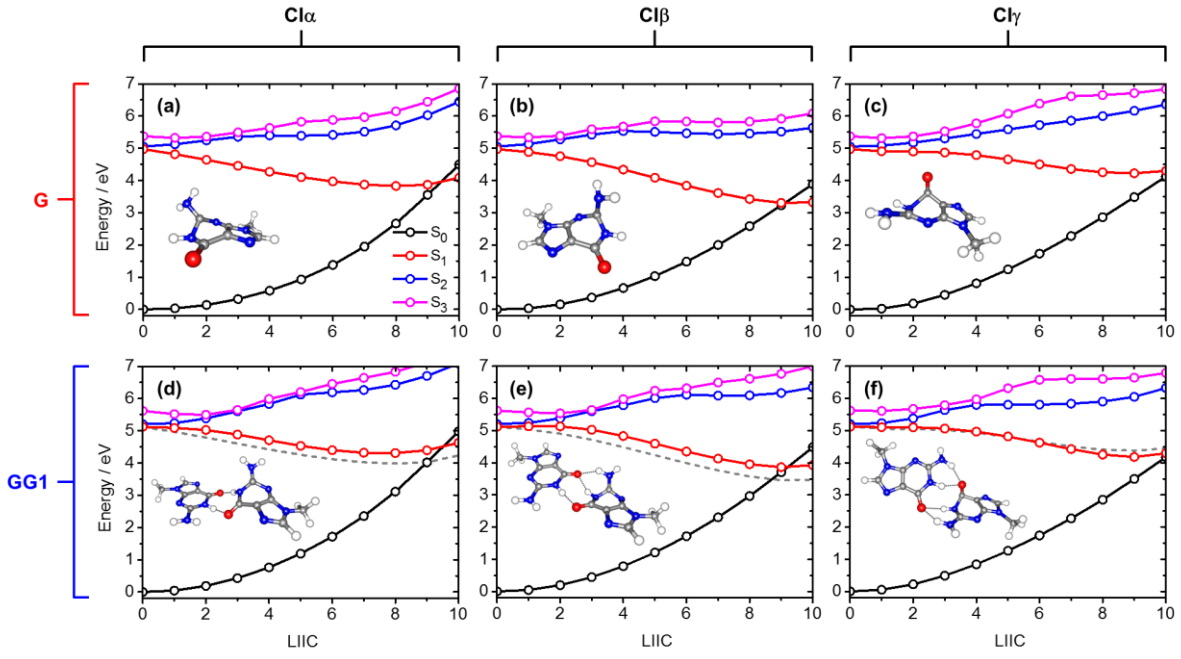

Fig. 8. Linear interpolations in internal coordinates (LIICs) from the S_0 minimum energy structures of the G monomer (**a-c**) and GG1 dimer (**d-f**) to respective conical intersections (CIα = left, CIβ =

middle and CIγ = right), returning adiabatic potential energy cuts for the singlet S_0 (black), S_1 (red), S_2 (blue) and S_3 (magenta) electronic states. Potential energy cuts were calculated at the ADC(2)/def2-TZVP and ADC(2)/def2-SVP levels of theory for G and GG1, respectively. Potential energy cuts of the G monomer S_1 state (shifted in energy so that S_1,G = S_1,GG1 at point 0) are shown for comparison to the profiles of the S_1 cuts of GG1 in panels d-f (grey dashed lines). Inset: conical intersection structures used in the LIICs, calculated at the SFTDDFT/BHHLYP/6-31g(d) level of theory.

In the transient spectroscopy measurements made in chloroform solution, we observe two time-constants of 210 fs and 2.6 ps contributing to the electronic deactivation of G. In the gas-phase dynamics simulations discussed above, guanine is predicted to undergo complete energetic deactivation to the electronic ground state within 1 ps. As chloroform is a non-coordinating solvent, it is expected to influence the relaxation dynamics mainly through electrostatic interactions and collisional deactivation. To investigate the effects of solvation computationally, we recalculated the same pathways using TDDFT including a chloroform PCM (SI Fig. S3), having benchmarked the TDDFT functional PW91 (SI Fig. S4) against the ADC(2) results discussed here, and found satisfactory agreement. The pathways for the first excited singlet state along the resulting LIICs are relatively unperturbed by the addition of the chloroform PCM for all three CIs.

On the basis of these and previous calculations, we suggest that the 210-fs time constant can be attributed to passage primarily via CIα, whereas the 2.6-ps time constant derives from a combination of excited state deactivations via CIβ and CIγ. A small solvent-induced distortion in the shapes of the potentials could be the origin of the longer time constant observed for decay via this latter channel in solution compared to the gas phase.

4.2 Dimer Relaxation Pathways

A MECI search for the 9-methyl-guanine dimer found several low-energy conical intersections with remarkable structural similarities to those calculated for the 9-methyl-guanine monomer. For the GG1 dimer CI structures, one G sub-unit remains planar and largely undistorted. The other G sub-unit of GG1 adopts structures which resemble those for the CIs discussed in section 4.1 for the G monomer, although the NH_2 group is not rotated in the same way as for the monomer at CIα. The exception is CIγ; on dimerization, this sub-unit also undergoes a large rotation to increase its coordination, and breaks the planar symmetry

present in the vFC region (SI Fig. S5). The distortion of only one of the G sub-units in the dimer at the CI region is perhaps surprising because the initial excitation is delocalized across both G units (Fig. 5), but it indicates that at least some of the energetic deactivation pathways in GG1 are monomer-like in nature.

The size of the GG1 dimer places heavy restrictions on a theoretical treatment of the system. A comparison of the effect of changing the basis size for the G monomer (SI Fig. S4) shows only a small energy offset between the triple-ζ and single-ζ basis sets, with the shape of the potentials being largely unchanged. For computational efficiency reasons, we are restricted to calculating the pathways from the Franck-Condon region to the CIs using ADC(2)/def2-SVP, but the comparison of basis sets for the G monomer suggests the shape of the potentials should be qualitatively unaffected by the reduction in basis set size.

Fig. 8 compares cuts through the calculated PESs from the vFC region to the three lowest-energy CI structures. On first inspection, the PESs appear largely unchanged by dimerization. For all three routes, the potentials in the immediate vicinity of the vFC region are slightly flatter than those calculated for the G monomer. The larger geometric distortion of the GG1 dimer at CIγ suggests that dimerization will have the greatest impact on the dynamics of this pathway. The small perturbation to the shape of the PES *en route* to CIβ may also be sufficient to promote greater branching of flux towards CIγ. There are no excited-state dynamical simulations for GG1 with which to compare our experimental measurements, and dynamical effects will undoubtedly play an important role, but given the similarities between the computed energetics of monomer and dimer pathways shown in Fig. 8, it is plausible that the measured 210-fs time-constant reflects energetic deactivation via CIα, just as argued for the monomer, and consistent with fluorescence lifetime measurements by Schwalb *et al*. [12], whereas the slightly longer time constant (τ_4 = 18 ps) represents a combination of the CIβ and CIγ pathways.

As well as the proposed monomer-like decay pathways, dimerization opens the possibility of other reaction channels including EDPT or hydrogen transfer, and it may modify the propensity for intersystem crossing to triplet states. For the monomer, the TVAS experiments show efficient repopulation of the ground state, and the short timescales involved suggest the need for strong singlet-triplet manifold interactions if ISC is to compete. While a full

theoretical exploration and discussion of these pathways is beyond the scope of this work, we highlight here some observations based on our results.

Recent experimental studies of thymidine photochemistry in chloroform [67], and prior work by Kohler and coworkers [73], showed that $^1n\pi^*$ states associated with the carbonyl groups acted as a doorway for population of a long-lived $^3\pi\pi^*$ state. An analogous mechanism may exist in GG1. Hunger *et al*. [32] proposed that the triplet state possessed $G^{\bullet+}G^{\bullet-}$ charge-transfer character, with a structured ESA signature arising from the $G^{\bullet+}$ radical cation in TEAS. Our calculations at the PW91/6-311+G** level indicate that, at its adiabatic minimum, the T_1 state of GG1 possesses strong $G^{\bullet+}G^{\bullet-}$ character. At this T_1 minimum, the C_{2h} symmetry is broken, which prevents conjugation of the π-system over the entire GG1 dimer, causing π-orbitals to localize onto individual G units, such that the spin-forbidden $T_1 \leftarrow S_0$ transition involves G(π) to G(π*) charge-transfer (with orbitals analogous to the HOMO and LUMO+2 of the G monomer). However, we do not observe structure characteristic of the absorption spectrum of $G^{\bullet+}$ in our TEAS measurements, suggesting that if triplet states are involved following GG1 photoexcitation in chloroform, they are not of $G^{\bullet+}G^{\bullet-}$ character.

Similar breaking of the planar symmetry is also indicated in the region of the S_1 minimum energy geometry for GG1, reminiscent of the MECI geometries reported in Fig. 8. This results in a similar localization of the electronic density onto one of the G subunits as was revealed by the T_1 state calculations. Previous theoretical investigations of hydrogen-transfer mechanisms in related heterodimers, with planar symmetry enforced on the excited state,[74-76] showed the hydrogen-transfer mechanisms to be mediated by such CT states. However, our preliminary calculations of these EDPT pathways in GG1 suggest they are too high in energy at both the vFC and S_{1min} region of the PES to contribute to our observed photochemical dynamics. Further computational investigation is required to explore fully the possibility of an EDPT mechanism.

5. Conclusions

In chloroform solution, the relaxation of UV-photoexcited $^1\pi\pi^*$-state homodimers (GG1) of the guanosine nucleoside follows two pathways also characteristic of the $^1\pi\pi^*$-state of the monomer G. Forces acting in the vertical Franck-Condon region of the $^1\pi\pi^*$ state direct the excited state nuclear dynamics along barrierless pathways, either towards a conical intersection CIα (a $^1\pi\pi^*/S_0$ CI involving pyramidalization at the C2/NH_2 site), or two conical intersections CIβ (a $^1\pi\pi^*/S_0$ CI with distortion of the NH_2 group) and CIγ (a $^1n\pi^*/S_0$ conical intersection with out-of-plane distortion of the C6=O carbonyl group). The 210 ± 20 fs time constant for relaxation via CIα is unchanged by dimerization, but the time constant attributed to the CIβ / CIγ pathway increases from 2.6 ± 0.1 ps in the monomer to 18 ± 2 ps in the GG1 dimer. Electronic structure calculations indicate that at conical intersections CIα and CIβ in the GG1 dimer, one G monomer unit distorts to a structure similar to that for the corresponding conical intersection in the isolated monomer, while the second G unit remains planar and undistorted. CIγ breaks the coplanarity of the two G units in the GG1 dimer. The gradients of the minimum energy pathways connecting the vertical Franck-Condon region to the conical intersections become slightly smaller in the dimers. A further, slower dynamical component with time constant 1.4 ± 0.6 ns, identified from the recovery of ground state GG1 molecules, is seen only in the homodimer. It may be indicative either of inter-base EDPT across the hydrogen bonds holding the two G units together, or intersystem crossing to the triplet manifold and subsequent relaxation of the T_1 state.

Acknowledgements

The experimental measurements at the University of Bristol were supported by ERC Advanced Grant 290966 CAPRI. KR gratefully acknowledges a postdoctoral fellowship from the Deutsche Forschungsgemeinschaft (DFG) R04951/1-1. The authors acknowledge the use of the EPSRC UK National Service for Computational Chemistry Software (NSCCS) at Imperial College London. The work at the University of Kiel was supported by DFG grant Te161/9-1 and the Collaborative Research Centre CRC 677. The Hokkaido University group thanks The Japan Science and Technology agency (JST) for support through grants JPMJPR16N8 and JPMJCR14L5. We are grateful to Dr Thomas Elsaesser, Dr Erik Nibbering and Dr Henk Fidder (Max Born Institute) for contributing to the 2D-IR measurements, and for valuable discussions.

Table 1. Degrees of association (β_{GG}) into GG dimers for different concentrations of G nucleosides in chloroform.

c_0 / mM	β_{GG}
1	0.50
1.5	0.57
7.7	0.78
10	0.80
100	0.93

Table 2. Calculated relative energies (ΔE), dissociation energies (D_e) and relative Boltzmann populations at 298 K (P_B) for the four H-bonded GG dimer structures in Fig. 1 (where R = CH_3).

	PCM-MP2/cc-pVDZ			PCM-SCS-MP2/cc-pVDZ			PCM-PW91/6-311+G**		
Dimer	ΔE / cm^{-1}	D_e / cm^{-1}	P_B(298 K)	ΔE / cm^{-1}	D_e / cm^{-1}	P_B(298 K)	ΔE / cm^{-1}	D_e / cm^{-1}	P_B(298 K)
GG1	0	6919	96.2 %	0	6086	92.6 %	0	5963	99.3 %
GG2	673	6246	3.7 %	529	5557	7.2 %	1035	4927	0.7 %
GG3	1537	5381	0.1 %	1314	4771	0.2 %	1763	4199	0 %
GG4	2751	4168	0 %	2576	3509	0 %	2939	3024	0 %

Table 3. Vertical excitation energies, oscillator strengths, orbital transitions (*cf*. Fig. 5) and state characters for the singlet excited states (S_n) of G and GG1 calculated at the ADC(2)/def2–TZVP and ADC(2)/def2–SVP levels of theory, respectively (H = HOMO, L = LUMO).

State	Character	Orbital Transition (%)	Vertical Energy / eV	Oscillator Strength, *f*
G				
S_1	ππ* (L_a)	H → L+1 (86)	4.97	0.2046
S_2	nπ*	H–2 → L+2 (47), H–4 → L+2 (19)	5.05	0.0003
S_3	ππ* (L_b)	H → L+2 (87)	5.37	0.2942
S_4	nπ*	H–2 → L+1 (64)	5.69	0.0000
S_5	πσ*	H → L (86)	5.90	0.0005
		GG1		
S_1	ππ*	H → L (38), H–1 → L+1 (22)	5.12	0.0000
S_2	ππ*	H–1 → L (39), H → L+1 (25)	5.21	0.2719
S_3	ππ*	H–1 → L+2 (34), H → L+3 (28)	5.62	0.9238
S_4	ππ*	H → L+2 (33), H–1 → L+3 (25)	5.68	0.0000

Table 4. Extracted time constant values (τ_n), their respective relative fit amplitudes A_n (scaled to sum to unity) and photophysical assignments, from a global fitting analysis of the experimental kinetic traces obtained from TEAS (Fig. 6; 1.5 mM solution) and TVAS (Fig. 7, 1 mM solution) measurements on G and GG1 in chloroform at 260 nm. Fit amplitudes for other probe wavelengths are reported in Table S1 of Supporting Information.

[a] Only resolved in TEAS on c_0 = 7.7 mM solutions; time constant τ_1 is an upper limit.

[b] A modified value of τ_4' = 19 ± 5 ps is required to fit the TVAS data.

		TEAS		TVAS				
Time Constant	Value	A_n (λ_{pr} = 340 nm)	A_n (λ_{pr} = 560 nm)	A_n ($\nu CO^{0\rightarrow2}/\delta sci^{0\rightarrow2}$)	A_n ($\nu NH_2 s$)	A_n (ν^*NH)	Species	Assignment
τ_1	70 ± 10 fs[a]	-1.76[a]	-	-	-	-	GG1	vFC SE
τ_2	210 ± 20 fs	-	0.78	-	-	-	G + GG1	$^1\pi\pi^*$ decay – CIα
τ_3	2.6 ± 0.1 ps	0.84	0.22	-	-	-	G	$^1\pi\pi^*$ decay – CIβ
τ_4	18 ± 2 ps[b]	0.16	-	0.36	-	0.04	GG1	$^1\pi\pi^*/^1n\pi^*$ decay – CIβ/CIγ
τ_5	6.7 ± 0.5 ps	-	-	0.28	1.00	0.73	G + GG1	S_0 vib. cooling
τ_6	1.4 ± 0.6 ns	-	-	0.36	-	0.23	GG1	T_1 decay or EDPT

References

[1] C.E. Crespo-Hernandez, B. Cohen, P.M. Hare, B. Kohler, Chem Rev 104 (2004) 1977.
[2] C.T. Middleton, K. de La Harpe, C. Su, Y.K. Law, C.E. Crespo-Hernandez, B. Kohler, Annu Rev Phys Chem 60 (2009) 217.
[3] M. Barbatti, A.J.A. Aquino, J.J. Szymczak, D. Nachtigallova, P. Hobza, H. Lischka, P Natl Acad Sci USA 107 (2010) 21453.
[4] R. Improta, F. Santoro, L. Blancafort, Chem Rev 116 (2016) 3540.
[5] W.J. Schreier, T.E. Schrader, F.O. Koller, P. Gilch, C.E. Crespo-Hernandez, V.N. Swaminathan, T. Carell, W. Zinth, B. Kohler, Science 315 (2007) 625.
[6] T. Zeleny, M. Ruckenbauer, A.J.A. Aquino, T. Muller, F. Lankas, T. Drsata, W.L. Hase, D. Nachtigallova, H. Lischka, J Am Chem Soc 134 (2012) 13662.
[7] C.E. Crespo-Hernandez, B. Cohen, B. Kohler, Nature 436 (2005) 1141.
[8] N.K. Schwalb, F. Temps, Science 322 (2008) 243.
[9] D.B. Bucher, A. Schlueter, T. Carell, W. Zinth, Angew Chem Int Edit 53 (2014) 11366.
[10] Y.Y. Zhang, K. de La Harpe, A.A. Beckstead, R. Improta, B. Kohler, J Am Chem Soc 137 (2015) 7059.
[11] K. Röttger, H.J.B. Marroux, M.P. Grubb, P.M. Coulter, H. Böhnke, A.S. Henderson, M.C. Galan, F. Temps, A.J. Orr-Ewing, G.M. Roberts, Angew Chem Int Edit 54 (2015) 14719.
[12] N.K. Schwalb, T. Michalak, F. Temps, J Phys Chem B 113 (2009) 16365.
[13] M. Gellert, M.N. Lipsett, D.R. Davies, P Natl Acad Sci USA 48 (1962) 2013.
[14] W. Guschlbauer, J.F. Chantot, D. Thiele, J Biomol Struct Dyn 8 (1990) 491.
[15] J.T. Davis, Angew Chem Int Edit 43 (2004) 668.
[16] J.R. Williamson, Annu Rev Bioph Biom 23 (1994) 703.
[17] E.H. Blackburn, Nature 350 (1991) 569.
[18] A. Gualberto, R.M. Patrick, K. Walsh, Gene Dev 6 (1992) 815.
[19] E. Henderson, C.C. Hardin, S.K. Walk, I. Tinoco, E.H. Blackburn, Cell 51 (1987) 899.
[20] R.J. Wellinger, D. Sen, Eur J Cancer 33 (1997) 735.
[21] J. Peon, A.H. Zewail, Chem Phys Lett 348 (2001) 255.
[22] J.M.L. Pecourt, J. Peon, B. Kohler, J Am Chem Soc 123 (2001) 10370.
[23] S. De Camillis, J. Miles, G. Alexander, O. Ghafur, I.D. Williams, D. Townsend, J.B. Greenwood, Phys Chem Chem Phys 17 (2015) 23643.
[24] H. Chen, S.H. Li, J Chem Phys 124 (2006) 154315.
[25] C.M. Marian, J Phys Chem A 111 (2007) 1545.
[26] S. Yamazaki, W. Domcke, A.L. Sobolewski, J Phys Chem A 112 (2008) 11965.
[27] S. Yamazaki, W. Domcke, J Phys Chem A 112 (2008) 7090.
[28] L. Serrano-Andres, M. Merchan, A.C. Borin, J Am Chem Soc 130 (2008) 2473.
[29] Z.G. Lan, E. Fabiano, W. Thiel, ChemPhysChem 10 (2009) 1225.
[30] M. Barbatti, J.J. Szymczak, A.J.A. Aquino, D. Nachtigallova, H. Lischka, J Chem Phys 134 (2011) 014304.
[31] K. Röttger, N.K. Schwalb, F. Temps, J Phys Chem A 117 (2013) 2469.
[32] K. Hunger, L. Buschhaus, L. Biemann, M. Braun, S. Kovalenko, R. Improta, K. Kleinermanns, Chem-Eur J 19 (2013) 5425.
[33] K.K. Ogilvie, Can J Chem 51 (1973) 3799.
[34] M.L. Cowan, B.D. Bruner, N. Huse, J.R. Dwyer, B. Chugh, E.T.J. Nibbering, T. Elsaesser, R.J.D. Miller, Nature 434 (2005) 199.

[35] M.L. Cowan, J.P. Ogilvie, R.J.D. Miller, Chem Phys Lett 386 (2004) 184.
[36] D. Kraemer, M.L. Cowan, A. Paarmann, N. Huse, E.T.J. Nibbering, T. Elsaesser, R.J.D. Miller, P Natl Acad Sci USA 105 (2008) 437.
[37] M. Yang, L. Szyc, K. Röttger, H. Fidder, E.T.J. Nibbering, T. Elsaesser, F. Temps, J Phys Chem B 115 (2011) 5484.
[38] K. Röttger, R. Siewertsen, F. Temps, Chem Phys Lett 536 (2012) 140.
[39] K. Röttger, S. Wang, F. Renth, J. Bahrenburg, F. Temps, Appl Phys B-Lasers 118 (2015) 185.
[40] G.M. Roberts, H.J.B. Marroux, M.P. Grubb, M.N.R. Ashfold, A.J. Orr-Ewing, J Phys Chem A 118 (2014) 11211.
[41] S. Grimme, J Chem Phys 118 (2003) 9095.
[42] J. Antony, S. Grimme, J Phys Chem A 111 (2007) 4862.
[43] J. Antony, S. Grimme, Phys Chem Chem Phys 8 (2006) 5287.
[44] M.J. Frisch, G.W. Trucks, H.B. Schlegel, G.E. Scuseria, M.A. Robb, J.R. Cheeseman, G. Scalmani, V. Barone, B. Mennucci, G.A. Petersson, H. Nakatsuji, M. Caricato, *Gaussian 09*; Gaussian Inc.: Wallingford, CT, 2009.
[45] R.A. Distasio, M. Head-Gordon, Mol Phys 105 (2007) 1073.
[46] J.P. Perdew, J.A. Chevary, S.H. Vosko, K.A. Jackson, M.R. Pederson, D.J. Singh, C. Fiolhais, Phys Rev B 46 (1992) 6671.
[47] T. van der Wijst, C.F. Guerra, M. Swart, F.M. Bickelhaupt, Chem Phys Lett 426 (2006) 415.
[48] J.A. Frey, A. Muller, M. Losada, S. Leutwyler, J Phys Chem B 111 (2007) 3534.
[49] Y. Zhao, D.G. Truhlar, Theor Chem Acc 120 (2008) 215.
[50] T. Yanai, D.P. Tew, N.C. Handy, Chem Phys Lett 393 (2004) 51.
[51] S. Maeda, T. Taketsugu, K. Ohno, K. Morokuma, J Am Chem Soc 137 (2015) 3433.
[52] S. Maeda, T. Taketsugu, K. Morokuma, J Comput Chem 35 (2014) 166.
[53] Y.H. Shao, M. Head-Gordon, A.I. Krylov, J Chem Phys 118 (2003) 4807.
[54] M.W. Schmidt, K.K. Baldridge, J.A. Boatz, S.T. Elbert, M.S. Gordon, J.H. Jensen, S. Koseki, N. Matsunaga, K.A. Nguyen, S.J. Su, T.L. Windus, M. Dupuis, J.A. Montgomery, J Comput Chem 14 (1993) 1347.
[55] S. Maeda, Y. Osada, Y. Harabuchi, T. Taketsugu, K. Morokuma, K. Ohno, GRRM, a developmental version, Hokkaido University, Sapporo, 2015.
[56] A.D. Becke, J Chem Phys 98 (1993) 1372.
[57] TURBOMOLE V7.0 2015, a development of University of Karlsruhe and Forschungszentrum Karlsruhe GmbH, 1989-2007, TURBOMOLE GmbH, since 2007; available from http://www.turbomole.com.
[58] C. Greve, N.K. Preketes, H. Fidder, R. Costard, B. Koeppe, I.A. Heisler, S. Mukamel, F. Temps, E.T.J. Nibbering, T. Elsaesser, J Phys Chem A 117 (2013) 594.
[59] H. Fidder, M. Yang, E.T.J. Nibbering, T. Elsaesser, K. Röttger, F. Temps, J Phys Chem A 117 (2013) 845.
[60] N.K. Schwalb, F. Temps, J Photoch Photobio A 208 (2009) 164.
[61] L. Biemann, T. Haber, D. Maydt, K. Schaper, K. Kleinermanns, J Chem Phys 128 (2008) 195103.
[62] E. Nir, C. Janzen, P. Imhof, K. Kleinermanns, M.S. de Vries, Phys Chem Chem Phys 4 (2002) 740.
[63] C. Greve, E.T.J. Nibbering, H. Fidder, J Phys Chem B 117 (2013) 15843.
[64] R. Costard, C. Greve, H. Fidder, E.T.J. Nibbering, J Phys Chem B 119 (2015) 2711.
[65] J.R. Platt, J Chem Phys 17 (1949) 484.

[66] A.L. Sobolewski, W. Domcke, Phys Chem Chem Phys 6 (2004) 2763.
[67] K. Röttger, H.J.B. Marroux, H. Böhnke, D.T.J. Morris, A.T. Voice, F. Temps, G.M. Roberts, A.J. Orr-Ewing, Faraday Discuss 194 (2016) 683
[68] D. Murdock, S.J. Harris, J. Luke, M.P. Grubb, A.J. Orr-Ewing, M.N.R. Ashfold, Phys Chem Chem Phys 16 (2014) 21271.
[69] J.J. Snellenburg, S.P. Laptenok, R. Seger, K.M. Mullen, I.H.M. van Stokkum, J Stat Softw 49 (2012) 1.
[70] H. Marciniak, S. Lochbrunner, Chem Phys Lett 609 (2014) 184.
[71] A.L. Sobolewski, W. Domcke, Chem Phys 294 (2003) 73.
[72] A. Padermshoke, Y. Katsumoto, R. Masaki, M. Aida, Chem Phys Lett 457 (2008) 232.
[73] P.M. Hare, C.T. Middleton, K.I. Mertel, J.M. Herbert, B. Kohler, Chem Phys 347 (2008) 383.
[74] T. Schultz, E. Samoylova, W. Radloff, I.V. Hertel, A.L. Sobolewski, W. Domcke, Science 306 (2004) 1765.
[75] S. Perun, A.L. Sobolewski, W. Domcke, J Phys Chem A 110 (2006) 9031.
[76] V. Sauri, J.P. Gobbo, J.J. Serrano-Perez, M. Lundberg, P.B. Coto, L. Serrano-Andres, A.C. Borin, R. Lindh, M. Merchan, D. Roca-Sanjuan, J Chem Theory Comput 9 (2013) 481.